

# Empirical Determination of Dark Matter Velocities using Metal-Poor Stars

Jonah Herzog-Arbeitman,<sup>1,\*</sup> Mariangela Lisanti,<sup>1,†</sup> Piero Madau,<sup>2,3,‡</sup> and Lina Necib<sup>4,§</sup>

<sup>1</sup>*Department of Physics, Princeton University, Princeton, NJ 08544, USA*

<sup>2</sup>*Department of Astronomy & Astrophysics, University of California, Santa Cruz, CA 95064, USA*

<sup>3</sup>*Institut d'Astrophysique de Paris, Sorbonne Universités, 75014 Paris, France*

<sup>4</sup>*Center for Theoretical Physics, Massachusetts Institute of Technology, Cambridge, MA 02139, USA*

The Milky Way dark matter halo is formed from the accretion of smaller subhalos. These subunits also harbor stars—typically old and metal-poor—that are deposited in the Galactic inner regions by disruption events. In this Letter, we show that the dark matter and metal-poor stars in the Solar neighborhood share similar kinematics due to their common origin. Using the high-resolution ERIS simulation, which traces the evolution of both the dark matter and baryons in a realistic Milky Way analog galaxy, we demonstrate that metal-poor stars are indeed effective tracers for the local, virialized dark matter velocity distribution. The dark matter velocities in the Solar neighborhood can therefore be inferred from observations of the smooth inner halo made by the Sloan Digital Sky Survey. This empirical distribution has a lower peak speed and smaller dispersion than what is typically assumed in the Standard Halo Model, affecting the interpretation of direct detection experiments. Specifically, the bounds on the spin-independent scattering cross section are weakened by nearly an order of magnitude for masses below  $\sim 10$  GeV. Upcoming data from *Gaia* will allow us to further refine the expected distribution for the smooth dark matter component, and to test for the presence of local substructure.

**Introduction.** The velocity distribution of dark matter (DM) in the Milky Way provides a fossil record of the galaxy’s evolutionary history. In the  $\Lambda$ CDM paradigm, the Milky Way’s DM halo forms from the hierarchical merger of smaller subhalos [1]. As a subhalo falls into, and then orbits, its host galaxy, it is tidally disrupted and continues to shed mass until it completely dissolves. With time, this tidal debris virializes and becomes smoothly distributed in phase space. Debris from more recent mergers that has not equilibrated can exhibit spatial or kinematic substructure [2–11].

Knowledge of the DM velocity distribution is required to interpret results from direct detection experiments [12, 13], which search for DM particles that scatter off terrestrial targets. The scattering rate in these experiments depends on both the local number density and velocity of the DM [14, 15]. In the Standard Halo Model (SHM), the velocity distribution is modeled as a Maxwell-Boltzmann, which assumes that the DM distribution is isotropic and in equilibrium [13]. Deviations from these assumptions can be important for certain classes of DM models (see [15] for a review).

$N$ -body simulations, which trace the build-up of Milky Way-like halos in a cosmological context, do find differences with the SHM. In DM-only simulations, this is most commonly manifested as an excess of high-velocity particles as compared to a Maxwellian distribution with the same peak velocity [16–18]. However, full hydrodynamic simulations, which include gas and stars, find that the presence of baryons makes the DM halos more spherical and the velocities more isotropic, consistent with the SHM [19–23].

In this Letter, we demonstrate that the DM velocity distribution can be empirically determined using populations of metal-poor stars in the Solar neighborhood.

This proposal relies on the fact that these old stars share a merger history with DM in the  $\Lambda$ CDM framework, and should therefore exhibit similar kinematics. The hierarchical formation of DM halos implies that the Milky Way’s stellar halo also formed from the accretion, and eventual disruption, of dwarf galaxies [24–29]. For example, the chemical abundance patterns of the stellar halo can be explained by the accretion—nearly 10 Gyr ago—of a few  $\sim 5 \times 10^{10} M_\odot$  DM halos hosting dwarf-irregular galaxies [30–32]. The stars from these accreted galaxies would have characteristic chemical abundances.

A star’s abundance of iron, Fe, and  $\alpha$ -elements (O, Ca, Mg, Si, Ti) depends on its host galaxy’s evolution. Core-collapse supernova (SN), like Type II, result in greater  $\alpha$ -enrichment relative to Fe over the order of a few Myr. Thermonuclear SN, such as Type Ia, however, act on longer time scales and produce large amounts of Fe relative to  $\alpha$  elements. For a galaxy that experiences only a brief star-formation period, the enrichment of its interstellar medium is dominated by explosions of core-collapse SN, suppressing Fe abundances. Observations indicate that the Milky Way’s inner stellar halo, which extends out to  $\sim 20$  kpc, is metal-poor, with an iron abundance of  $[Fe/H] \sim -1.5$  and  $\alpha$ -enhancement of  $[\alpha/Fe] \sim 0.3$  [33–38].<sup>1</sup>

To demonstrate the correlation between the stellar and DM velocity distributions, we use the ERIS simulation, one of the highest resolution hydrodynamic simulations

<sup>1</sup> The stellar abundance of element  $X$  relative to  $Y$  is defined as:

$$[X/Y] = \log_{10} (N_X/N_Y) - \log_{10} (N_X/N_Y)_\odot,$$

where  $N_i$  is the number density of the  $i^{\text{th}}$  element.

of a Milky Way–like galaxy [39]. We show that the velocity distribution of metal-poor halo stars in ERIS successfully traces that of the virialized DM component in the Solar neighborhood. Using results from the Sloan Digital Sky Survey (SDSS), we then infer the local velocity distribution for the smooth DM component in our Galaxy. The result differs from the SHM in important ways, and suggests that current limits on spin-independent DM may be too strong for masses below  $\sim 10$  GeV.

**The ERIS Simulation.** ERIS is a cosmological zoom-in simulation that employs smoothed particle hydrodynamics to model the DM, gas, and stellar distributions in a Milky Way–like galaxy from  $z = 90$  to today [39, 40]. It employs the TreeSPH code GASOLINE [41] to simulate the evolution of the galaxy in a WMAP cosmology [42]. The mass resolution is  $9.8 \times 10^4$  and  $2 \times 10^4 M_\odot$  for each DM and gas ‘particle,’ respectively. An overview of the simulation is provided in Refs. [39, 40, 43–45], and we summarize the relevant aspects for our study here.

The ERIS DM halo has a virial mass of  $M_{\text{vir}} = 7.9 \times 10^{11} M_\odot$  and radius  $R_{\text{vir}} = 239$  kpc, and experienced no major mergers after  $z = 3$ . Within  $R_{\text{vir}}$ , there are  $7 \times 10^6$ ,  $3 \times 10^6$ , and  $8.6 \times 10^6$  DM, gas, and star particles, respectively. At  $z = 0$ , the DM halo hosts a late-type spiral galaxy. The disk has a scale length of 2.5 kpc and exponential scale height of 490 pc at 8 kpc from the galactic center. The properties of the ERIS disk and halo are comparable to their Milky Way values [39, 43]

A star ‘particle’ of mass  $6 \times 10^3 M_\odot$  is produced if the local gas density exceeds 5 atoms/cm<sup>3</sup>. The star formation rate depends on the gas density,  $\rho_{\text{gas}}$ , as  $d\rho_*/dt = 0.1 \rho_{\text{gas}}/t_{\text{dyn}} \propto \rho_{\text{gas}}^{1.5}$ , where  $\rho_*$  is the stellar density and  $t_{\text{dyn}}$  is the dynamical time. Metals are redistributed by stellar winds and Type Ia and Type II SNe [44, 45]. The abundances of Fe and O are tracked as the simulation evolves, while the abundances of all other elements are extrapolated assuming their measured solar values [46]. The Supplementary Material provides a detailed explanation for the chemical abundance modeling in ERIS.

Stars may either be bound to the main host halo or to its satellites when they form. We are primarily interested in the latter, as these stars share a common origin with the DM. The vast majority of halo stars in ERIS originated in satellites and are older than those born in the host [43]. They are more metal-poor than disk stars, on average, and we take advantage of this difference to distinguish the two components in the ERIS galaxy.

**Stellar Tracers for Dark Matter.** Figure 1 shows the density distribution of the DM and stars in ERIS as a function of Galactocentric radius. The distribution for all stars is steeper than that for DM. However, this includes contributions from thin and thick disk, as well as halo stars. To select the stars that are most likely to be members of the halo, we place cuts on both the Fe and  $\alpha$ -element abundances. Figure 1 illustrates what happens when progressively stronger cuts are placed on

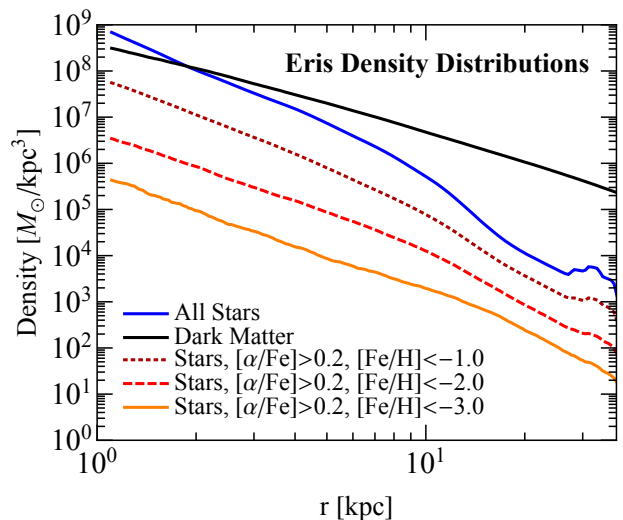


FIG. 1: The density distribution as a function of Galactocentric radius for the dark matter (black) and all stars (blue) in ERIS. The distributions for subsamples of stars with  $[\alpha/\text{Fe}] > 0.2$  and  $[\text{Fe}/\text{H}] < -1, -2, -3$  are also shown (dotted brown, dashed red, and solid orange, respectively). The density of the most metal-poor stellar population exhibits the same dependence on radius as the dark matter near the Sun’s position,  $r_\odot \sim 8$  kpc.

$[\text{Fe}/\text{H}]$ , while keeping  $[\alpha/\text{Fe}] > 0.2$ . As the cut on iron abundance varies from  $[\text{Fe}/\text{H}] < -1$  to  $[\text{Fe}/\text{H}] < -3$ , the density fall-off becomes noticeably more shallow.

Because the focus of this work is the DM distribution in the Solar neighborhood, we consider galactocentric radii in the range  $|r - r_\odot| \leq 2$  kpc, where  $r_\odot = 8$  kpc is the Sun’s position. In this range, the DM distribution falls off as  $\rho(r) \propto r^{-2.07 \pm 0.01}$ , which is essentially consistent with the best-fit power-law for the most metal-poor subsample, which falls off as  $\rho(r) \propto r^{-2.24 \pm 0.12}$ . This illustrates that the stars with lower iron abundance are adequate tracers for the underlying DM density distribution (see also Ref. [49]). The correspondence between the density distributions breaks down above  $r \gtrsim 20$  kpc, indicating a transition from the inner to the outer halo that is consistent with observations [47].

Figure 2 compares the velocity distribution of candidate halo stars in ERIS with that of the DM.<sup>2</sup> For comparison, we also show the stellar distribution with no metallicity cuts; it is dominated by disk stars with a characteristic peak at  $v_\phi \simeq 220$  km/s and narrow dispersions in the radial and vertical directions. All distributions are shown for  $|r - r_\odot| \leq 2$  kpc. Because direct detection experiments are only sensitive to DM within the Solar neighborhood, we restrict its vertical displacement from the disk to be  $|z_{\text{DM}}| \leq 2$  kpc. The stellar distributions are

<sup>2</sup> Throughout, we define the  $z$ -axis to be oriented along the angular momentum vector of the stars.

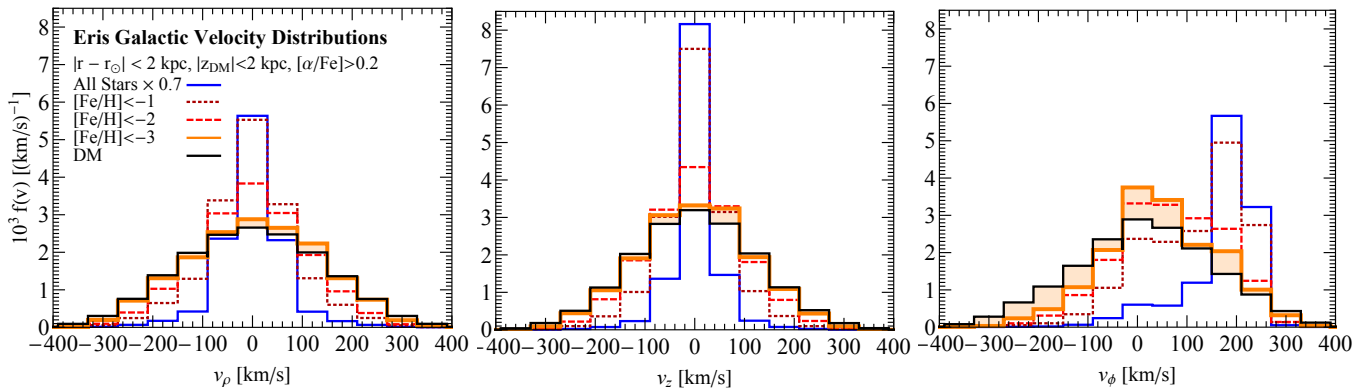


FIG. 2: Distributions of the three separate velocity components of the DM (solid black) and stars in ERIS. The velocities are in the galactocentric frame, where the  $z$ -axis is oriented along the stellar angular momentum vector. The stellar distributions are shown separately for different metallicities, with  $[\alpha/\text{Fe}] > 0.2$  and iron abundance varying from  $[\text{Fe}/\text{H}] < -1$  (dotted brown) to  $[\text{Fe}/\text{H}] < -3$  (solid orange). The distribution for all stars—dominated primarily by the disk—is also shown (solid blue). All distributions are shown for  $|r - r_\odot| \leq 2$  kpc; the DM is additionally required to lie within 2 kpc of the plane. To guide the eye, the orange shading highlights the differences between the DM and  $[\text{Fe}/\text{H}] < -3$  distributions. The discrepancy in the  $v_\phi$  distributions is due to the preferential disruption of subhalos on prograde orbits in ERIS; observations of the Milky Way halo do not see such pronounced prograde rotation [47, 48].

shown with no cut on the vertical displacement; we find that the results do not change if we restrict the metal-poor population to vertical displacements greater than 2 kpc. Unfortunately, there are too few metal-poor star particles within 2 kpc of the disk in ERIS to restrict to this region.

The  $v_\rho$  and  $v_z$  distributions show an excellent correspondence between the halo stars and the DM. Indeed, as increasingly more metal-poor stars are selected, their velocity distribution approaches that of the DM exactly. We apply the two-sided Kolmogorov-Smirnov test to establish whether the DM and halo stars share the same  $v_\rho$  and  $v_z$  probability distributions. The null hypothesis that the DM and stars share the same parent distribution is rejected at 95% confidence if the  $p$ -value is less than 0.05. The  $p$ -values for the  $(v_\rho, v_z)$  distributions are (0.9, 0.1) for  $[\text{Fe}/\text{H}] < -3$ , suggesting that its velocity distribution is indistinguishable from that of the DM in the radial and vertical directions.

Interpreting the distribution of azimuthal velocities requires more care. As illustrated in Fig. 2, the azimuthal velocities are skewed to positive values for both the DM and halo stars. The prograde rotation in the DM distribution is attributable to the ‘dark disk,’ which comprises  $\sim 9\%$  of all the DM in the Solar neighborhood in ERIS [43]. Dark disks form from the disruption of subhalos as they pass through the galactic disk. Subhalos on prograde orbits are preferentially disrupted due to dynamical friction, leading to a co-rotating DM disk [50]. The effect on the stars is similar, and—indeed—more pronounced due to dissipative interactions between halo stars and the disk [43]. The end result is that the halo stars systematically under-predict the DM distribution at negative azimuthal velocities.

Current observations suggest that our own Milky Way

has an inner halo with either modest or vanishing prograde rotation [47, 48], and constrain the possible contributions from a dark disk [51]. This suggests that the mergers that resulted in ERIS’ prograde halo might not have occurred in our own Galaxy, making the comparison of the DM and halo azimuthal motions more straightforward in realization. In the absence of such mergers, we assume that the DM and metal-poor stars have  $v_\phi$  distributions that match just as well as those in the  $v_\rho$  and  $v_z$  cases.

We have verified that the results presented in Fig. 2 are robust even as the spatial and  $[\alpha/\text{Fe}]$  cuts are varied. We consider  $[\alpha/\text{Fe}] \in [0.2, 0.4]$ , remove the  $[\alpha/\text{Fe}]$  cut altogether, and study the region where  $|r - r_\odot| \leq 1$  kpc. In all these cases, the conclusions remain the same.

**Empirical Velocity Distribution.** We now look to the kinematic properties of the Milky Way’s inner halo to infer the local DM velocities by extrapolating the correspondence argued above to our Galaxy. Spatial, chemical, and kinematic properties of the smooth inner halo have been characterized by SDSS [38, 48, 52]. The sample includes stars with  $r$ -band magnitude  $r < 20$  and heliocentric distances of  $\sim 100$  pc to 10 kpc that cover  $6500 \text{ deg}^2$  of sky at latitudes  $|b| > 20^\circ$  [48]. The metallicity of the the halo stars is well-modeled by a Gaussian with mean  $[\text{Fe}/\text{H}] = -1.46$  and standard deviation 0.30 dex [52]. The Galactic velocity distribution is provided for candidate halo stars with  $[\text{Fe}/\text{H}] < -1.1$ :

$$f(\mathbf{v}) = \frac{1}{(2\pi)^{3/2} \sigma_r \sigma_\theta \sigma_\phi} \exp \left[ -\frac{v_r^2}{2\sigma_r^2} - \frac{v_\theta^2}{2\sigma_\theta^2} - \frac{v_\phi^2}{2\sigma_\phi^2} \right], \quad (1)$$

where  $\{\sigma_r, \sigma_\phi, \sigma_\theta\} = \{141, 85, 75\} \pm 5$  km/s in spherical coordinates. Over the volume probed, the velocity ellipsoid does not exhibit a tilt in the spherical coordinate

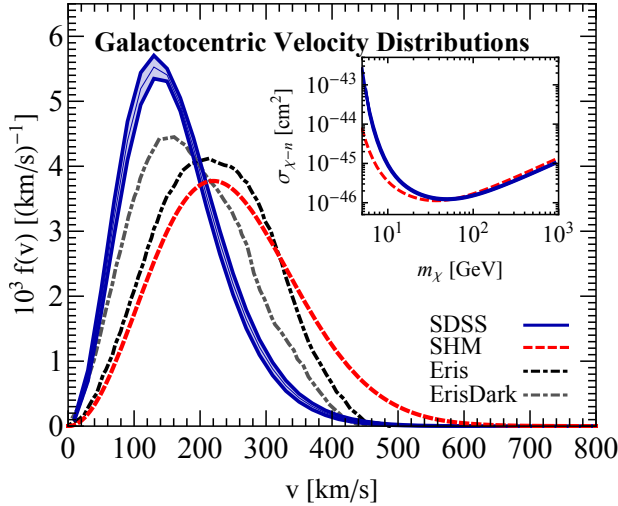


FIG. 3: Galactocentric speed distribution for SDSS inner-halo stars (solid blue), generated from Eq. 1. For comparison, we show the Standard Halo Model (dashed red), and the dark matter speed distributions in the ERIS (dot-dashed black) and ERISDARK halos (dot-dashed gray). The inset shows the expected background-free 95% C.L. limit on the DM spin-independent scattering cross section, assuming the exposure and energy threshold of the LUX experiment [53] for the SDSS and SHM velocity distributions.

system and the dispersions are constant. Additionally, the azimuthal velocities (in cylindrical coordinates) exhibit no prograde motion, in contrast to ERIS.

Figure 3 shows the speed distribution for a mock catalog of halo stars generated using Eq. 1, with a spread that corresponds to varying the dispersions within their  $1\sigma$  errors. The peak velocity is located at  $\sim 130$  km/s. For comparison, the ERIS DM speed distribution is shown for the region  $|r - r_\odot| \leq 2$  kpc and  $|z_{\text{DM}}| \leq 2$  kpc. ERISDARK is a DM-only simulation generated with the same initial conditions as ERIS and described in Ref. [20]; its DM speed distribution, plotted for  $|r - r_\odot| \leq 2$  kpc, is included as an example of a DM-only simulation result, which typically yields lower peak speeds. For comparison, the SHM is also included in Fig. 3. For an isotropic dispersion ( $\sigma = \sigma_{r,\phi,\theta}$ ), Eq. 1 simplifies to the Maxwell-Boltzmann distribution  $f(v) \propto e^{-v^2/2\sigma^2}$ . This corresponds to a collisionless isothermal distribution with density  $\rho(r) \propto r^{-2}$ , and yields a flat rotation curve with circular velocity  $v_c^2 = 2\sigma^2$ , where  $v_c \sim 220$  km/s.

If the SDSS halo stars are adequate tracers for the local DM, then Fig. 3 suggests that the DM speeds may be slower, on average, than what is expected in the SHM. This can lead to noticeable differences in the predicted signal rate for direct detection experiments. If a DM particle of mass  $m_\chi$  scatters off a nucleus with momentum transfer  $q$  and effective cross section  $\sigma(q^2)$ , the scattering

rate is

$$\frac{dR}{dE_{\text{nr}}} = \frac{\rho_\chi}{2m_\chi\mu} \sigma(q^2) F(q) \int_{v_{\text{min}}}^{\infty} \frac{f(\mathbf{v} + \mathbf{v}_{\text{obs}}(t))}{v} d^3v, \quad (2)$$

where  $E_{\text{nr}}$  is the recoil energy of the nucleus,  $\rho_\chi$  is the local DM density,  $\mu$  is the DM-nucleus reduced mass,  $F(q)$  is the exponential nuclear form factor [14],  $v_{\text{min}}$  is the minimum velocity needed to scatter, and  $\mathbf{v}_{\text{obs}}(t)$  is the velocity of the lab frame relative to the Galactic frame. Assuming the exposure of the LUX experiment, with  $3.35 \times 10^4$  kg days and a minimum energy threshold of 1.1 keV [53], we derive the 95% one-sided Poisson C.L. bound (3.0 events) on the scattering cross section as a function of the DM mass. The result is shown in the inset of Fig. 3 for the SHM and SDSS distributions. The bounds on the lightest DM are significantly weakened when the empirical distribution is used rather than the SHM.

There are several important caveats to keep in mind. First, the SDSS distribution is obtained for candidate halo stars with  $[\text{Fe}/\text{H}] < -1.1$ , and we have yet to demonstrate that these truly probe the kinematics of the primordial population of the halo. To achieve this, we must understand how the distribution evolves as progressively tighter cuts are placed on the iron abundance. If the distribution remains stable, then we can feel confident in extrapolating the results to DM based on the intuition garnered from ERIS. Second, Eq. 1 only describes the *smooth* component of the inner halo in the SDSS volume, and does not account for any spatial or kinematic substructure.

**Conclusions.** In this Letter, we propose that DM velocities can be determined empirically using metal-poor stars in the Solar neighborhood. Low metallicity stars are typically born in galaxies outside our own. Like DM, they are dragged into the Milky Way through mergers, and predominantly populate the halo surrounding the disk. We demonstrate the close correlation between the distributions of DM and metal-poor stars using the ERIS simulation, and conclude that the kinematics of the primordial stellar population tracks that of the virialized DM. To verify the generality of these findings and understand their dependence on the merger history, this study should be repeated with other hydrodynamic simulations of Milky Way-like halos. It would also be pertinent to understand whether the correspondence holds in generalizations of  $\Lambda$ CDM, such as self-interacting DM.

The velocity distribution of the smooth inner halo has been characterized by SDSS and can be used to infer the local DM velocities. The corresponding speed distribution has a lower peak velocity and smaller dispersion than what is typically assumed in the SHM. This affects predictions for the DM scattering rate in direct detection experiments. Specifically, the empirical DM distribution weakens published limits on the spin-independent cross section by nearly an order of magnitude at masses below



$\sim 10$  GeV. The wealth of data from *Gaia* [54] will allow us to better understand whether the SDSS distribution is an accurate descriptor of the most metal-poor stars in the Solar neighborhood, and whether any additional substructure exists from recent mergers. We explore this subject in greater detail in a follow-up study [55].

**Acknowledgements.** We thank George Brova, David Hogg, Nick Gnedin, Alexander Ji, Mario Jurić, Adrian Price-Whelan, and Željko Ivezić for helpful conversations. M.L. is supported by the DOE under contract DESC0007968, as well as by the Alfred P. Sloan Foundation. P.M. thanks the Préfecture of the Ile-de-France Region through the award of a Blaise Pascal International Research Chair, managed by the Fondation de l'Ecole Normale Supérieure. L.N. is supported by the DOE under contract DESC00012567.

---

\* Electronic address: [jonahh@princeton.edu](mailto:jonahh@princeton.edu)

† Electronic address: [mlisanti@princeton.edu](mailto:mlisanti@princeton.edu)

‡ Electronic address: [pmadau@ucolick.org](mailto:pmadau@ucolick.org)

§ Electronic address: [lhecib@mit.edu](mailto:lhecib@mit.edu)

- [1] L. Searle and R. Zinn, *Astrophys. J.* **225**, 357 (1978).
- [2] J. S. Bullock and K. V. Johnston, *Astrophys. J.* **635**, 931 (2005), [astro-ph/0506467](#).
- [3] A. P. Cooper et al., *Mon. Not. R. Astron. Soc.* **406**, 744 (2010), 0910.3211.
- [4] A. Helmi, A. P. Cooper, S. D. M. White, S. Cole, C. S. Frenk, and J. F. Navarro, *Astrophys. J. Lett.* **733**, L7 (2011), 1101.2544.
- [5] A. Kewley, H. L. Morrison, A. Helmi, T. D. Kinman, J. Van Duyne, J. C. Martin, P. Harding, J. E. Norris, and K. C. Freeman, *Astron. J.* **134**, 1579 (2007), 0707.4477.
- [6] H. L. Morrison et al., *Astrophys. J.* **694**, 130 (2009), 0804.2448.
- [7] M. C. Smith, N. W. Evans, V. Belokurov, P. C. Hewett, D. M. Bramich, G. Gilmore, M. J. Irwin, S. Vidrih, and D. B. Zucker, *Mon. Not. R. Astron. Soc.* **399**, 1223 (2009), 0904.1012.
- [8] R. J. Klement, *Astron. Astrophys. Rev.* **18**, 567 (2010), 1007.3257.
- [9] M. Lisanti and D. N. Spergel, *Phys. Dark Univ.* **1**, 155 (2012), 1105.4166.
- [10] M. Kuhlen, M. Lisanti, and D. N. Spergel, *Phys. Rev. D* **86**, 063505 (2012), 1202.0007.
- [11] M. Lisanti, L. E. Strigari, J. G. Wacker, and R. H. Wechsler, *Phys. Rev. D* **83**, 023519 (2011), 1010.4300.
- [12] M. W. Goodman and E. Witten, *Phys. Rev. D* **31**, 3059 (1985).
- [13] A. K. Drukier, K. Freese, and D. N. Spergel, *Phys. Rev. D* **33**, 3495 (1986).
- [14] G. Jungman, M. Kamionkowski, and K. Griest, *Phys. Rep.* **267**, 195 (1996), [hep-ph/9506380](#).
- [15] K. Freese, M. Lisanti, and C. Savage, *Rev. Mod. Phys.* **85**, 1561 (2013), 1209.3339.
- [16] M. Vogelsberger, A. Helmi, V. Springel, S. D. M. White, J. Wang, C. S. Frenk, A. Jenkins, A. D. Ludlow, and J. F. Navarro, *Mon. Not. Roy. Astron. Soc.* **395**, 797 (2009), 0812.0362.
- [17] J. March-Russell, C. McCabe, and M. McCullough, *JHEP* **05**, 071 (2009), 0812.1931.
- [18] M. Kuhlen, N. Weiner, J. Diemand, P. Madau, B. Moore, D. Potter, J. Stadel, and M. Zemp, *JCAP* **1002**, 030 (2010), 0912.2358.
- [19] F. S. Ling, E. Nezri, E. Athanassoula, and R. Teyssier, *JCAP* **1002**, 012 (2010), 0909.2028.
- [20] A. Pillepich, M. Kuhlen, J. Guedes, and P. Madau, *Astrophys. J.* **784**, 161 (2014), 1308.1703.
- [21] N. Bozorgnia et al., *JCAP* **1605**, 024 (2016), 1601.04707.
- [22] C. Kelso, C. Savage, M. Valluri, K. Freese, G. S. Stinson, and J. Bailin, *JCAP* **1608**, 071 (2016), 1601.04725.
- [23] J. D. Sloane, M. R. Buckley, A. M. Brooks, and F. Governato (2016), 1601.05402.
- [24] L. Searle and R. Zinn, *Astrophys. J.* **225**, 357 (1978).
- [25] K. V. Johnston, L. Hernquist, and M. Bolte, *Astrophys. J.* **465**, 278 (1996), [astro-ph/9602060](#).
- [26] A. Helmi, S. D. M. White, P. T. de Zeeuw, and H.-S. Zhao, *Nature* **402**, 53 (1999), [astro-ph/9911041](#).
- [27] A. Helmi and S. D. M. White, *Mon. Not. Roy. Astron. Soc.* **307**, 495 (1999), [astro-ph/9901102](#).
- [28] J. S. Bullock, A. V. Kravtsov, and D. H. Weinberg, *Astrophys. J.* **548**, 33 (2001), [astro-ph/0007295](#).
- [29] J. S. Bullock and K. V. Johnston, *Astrophys. J.* **635**, 931 (2005), [astro-ph/0506467](#).
- [30] B. Robertson, J. S. Bullock, A. S. Font, K. V. Johnston, and L. Hernquist, *Astrophys. J.* **632**, 872 (2005), [astro-ph/0501398](#).
- [31] A. S. Font, K. V. Johnston, J. S. Bullock, and B. Robertson, *Astrophys. J.* **638**, 585 (2006), [astro-ph/0507114](#).
- [32] A. S. Font, K. V. Johnston, J. S. Bullock, and B. E. Robertson, *Astrophys. J.* **646**, 886 (2006), [astro-ph/0512611](#).
- [33] S. G. Ryan and J. E. Norris, *Astron. J.* **101**, 1835 (1991).
- [34] S. G. Ryan and J. E. Norris, *Astron. J.* **101**, 1865 (1991).
- [35] A. McWilliam, G. W. Preston, C. Sneden, and L. Searle, *Astron. J.* **109**, 2757 (1995).
- [36] C. Allende Prieto, T. C. Beers, R. Wilhelm, H. J. Newberg, C. M. Rockosi, B. Yanny, and Y. S. Lee, *Astrophys. J.* **636**, 804 (2006), [astro-ph/0509812](#).
- [37] K. A. Venn, M. Irwin, M. D. Shetrone, C. A. Tout, V. Hill, and E. Tolstoy, *Astron. J.* **128**, 1177 (2004), [astro-ph/0406120](#).
- [38] Z. Ivezić et al. (SDSS), *Astrophys. J.* **684**, 287 (2008), 0804.3850.
- [39] J. Guedes, S. Callegari, P. Madau, and L. Mayer, *Astrophys. J.* **742**, 76 (2011), 1103.6030.
- [40] J. Guedes, L. Mayer, M. Carollo, and P. Madau, *Astrophys. J.* **772**, 36 (2013), 1211.1713.
- [41] J. W. Wadsley, J. Stadel, and T. R. Quinn, *New Astron.* **9**, 137 (2004), [astro-ph/0303521](#).
- [42] D. N. Spergel et al. (WMAP), *Astrophys. J. Suppl.* **170**, 377 (2007), [astro-ph/0603449](#).
- [43] A. Pillepich, P. Madau, and L. Mayer, *Astrophys. J.* **799**, 184 (2015), 1407.7855.
- [44] S. Shen, G. Kulkarni, P. Madau, and L. Mayer (2016), 1612.02832.
- [45] S. Shen, R. J. Cooke, E. Ramirez-Ruiz, P. Madau, L. Mayer, and J. Guedes, *Astrophys. J.* **807**, 115 (2015), 1407.3796.
- [46] M. Asplund, N. Grevesse, A. J. Sauval, and P. Scott, *Ann. Rev. Astron. Astrophys.* **47**, 481 (2009), 0909.0948.
- [47] D. Carollo et al., *Nature* **450**, 1020 (2007), 0706.3005.
- [48] N. A. Bond et al. (SDSS), *Astrophys. J.* **716**, 1 (2010),

- 0909.0013.
- [49] P. B. Tissera and C. Scannapieco, *Mon. Not. Roy. Astron. Soc.* **445**, 21 (2014), 1407.5800.
  - [50] J. I. Read, G. Lake, O. Agertz, and V. P. Debattista (2008), 0803.2714.
  - [51] J. I. Read, *J. Phys.* **G41**, 063101 (2014), 1404.1938.
  - [52] M. Juric et al. (SDSS), *Astrophys. J.* **673**, 864 (2008), astro-ph/0510520.
  - [53] D. S. Akerib et al. (LUX), *Phys. Rev. Lett.* **118**, 021303 (2017), 1608.07648.
  - [54] M. A. C. Perryman et al., *Astron. Astrophys.* **369**, 339 (2001), astro-ph/0101235.
  - [55] J. Herzog-Arbeitman, M. Lisanti, and L. Necib, *In Preparation* (2017).
  - [56] C. M. Raiteri, M. Villata, and J. F. Navarro, *Astron. Astrophys.* **315**, 105 (1996).
  - [57] P. Kroupa, C. A. Tout, and G. Gilmore, *Mon. Not. Roy. Astron. Soc.* **262**, 545 (1993).
  - [58] S. E. Woosley and T. A. Weaver, *Astrophys. J. Suppl.* **101**, 181 (1995).
  - [59] F.-K. Thielemann, K. Nomoto, and K. Yokoi, *Astron. Astrophys.* **158**, 17 (1986).
  - [60] G. Chabrier, *Astrophys. J. Lett.* **586**, L133 (2003), astro-ph/0302511.
  - [61] S. E. Woosley and A. Heger, *Physics Reports* **442**, 269 (2007), astro-ph/0702176.
  - [62] K. Iwamoto, F. Brachwitz, K. Nomoto, N. Kishimoto, H. Umeda, W. R. Hix, and F.-K. Thielemann, *Astrophys. J. Suppl.* **125**, 439 (2000), astro-ph/0002337.
  - [63] J.-h. Kim et al. (AGORA), *Astrophys. J. Suppl.* **210**, 14 (2013), 1308.2669.
  - [64] D. Maoz, F. Mannucci, and T. D. Brandt, *Mon. Not. R. Astron. Soc.* **426**, 3282 (2012), 1206.0465.

## Supplementary Material

This Supplementary Material reviews how the chemical abundances are determined in the ERIS simulation [39, 40, 44, 45]. The Fe and O yields depend on both the initial mass function (IMF), which sets the number of Type Ia and II supernovae (SNe), as well as the assumed chemical yields from each. The ERIS yields are obtained following a procedure similar to that of Ref. [56]. Each  $M_s = 6 \times 10^3 M_\odot$  stellar particle in ERIS represents its own population of stars. The distribution of masses for the particle’s constituents are set by the Kroupa (1993) IMF [57]:

$$\Phi_{\text{Kroupa}}(m) = M_s \times N_K \times \begin{cases} 2^{0.9} m^{-1.3} & 0.08 \leq m < 0.5 M_\odot \\ m^{-2.2} & 0.5 \leq m < 1 M_\odot \\ m^{-2.7} & m \geq 1 M_\odot, \end{cases} \quad (\text{S1})$$

where  $m$  is the stellar mass in units of  $M_\odot$  and  $N_K = 0.303$  is a normalization constant chosen such that  $\int m \Phi_{\text{Kroupa}} dm = M_s M_\odot$  for  $0.08 \leq m \leq 100 M_\odot$ .

Stars with masses between 8 and 40  $M_\odot$  explode as Type II SN, depositing iron and oxygen with mass yields

$$\begin{aligned} M_{\text{Fe}} &= 2.802 \times 10^{-4} m^{1.864} M_\odot \\ M_{\text{O}} &= 4.586 \times 10^{-4} m^{2.721} M_\odot, \end{aligned} \quad (\text{S2})$$

which follow the parametrization of Ref. [58]. Determining the number of Type Ia SN that are produced is more involved—see Ref. [56] for a full description. Each Type Ia SN produces 0.63  $M_\odot$  and 0.13  $M_\odot$  of Fe and O, respectively [59].

Using the IMF and yields described above, we find that a single star particle in ERIS produces 29.2 and 4.68 Type II and Ia SNe, respectively. This results in 1.32  $M_\odot$  of Fe and 28.5  $M_\odot$  of O from Type II SN, as well as 2.95  $M_\odot$  of Fe and 0.608  $M_\odot$  of O from Type Ia SN.

The relative contribution of Fe and O depends on the assumptions made for the IMF and mass yields. Let us consider how these values change taking the more modern Chabrier (2003) IMF [60] and the mass yields of Ref. [61, 62]. This follows the prescription used for the AGORA project [63]. The Chabrier mass function is

$$\Phi_{\text{Chabrier}}(m) = M_s \times N_C \times \begin{cases} m^{-1} e^{-(\log m - \log m_c)^2 / 2\sigma^2} & m < 1 M_\odot \\ 0.283 m^{-2.3} & m \geq 1 M_\odot, \end{cases} \quad (\text{S3})$$

where  $m_c = 0.08 M_\odot$ ,  $\sigma = 0.69$ , and the normalization  $N_C = 0.843$  is chosen such that  $\int m \Phi_{\text{Chabrier}} dm = 1 M_\odot$  for  $0.1 \leq m \leq 100 M_\odot$ . In this case, 64.7 and 10.4 Type II and Ia SNe are produced per star particle, respectively. This assumes that the SN Ia rate is 14% of the total, in agreement with recent estimates by Ref. [64]. The iron and oxygen yields for a Type II explosion are

$$\begin{aligned} M_{\text{Fe}} &= 0.375 e^{-17.94/m} M_\odot \\ M_{\text{O}} &= 27.66 e^{-51.81/m} M_\odot, \end{aligned} \quad (\text{S4})$$

whereas a Type Ia SN produces 0.63  $M_\odot$  and 0.14  $M_\odot$  of Fe and O, respectively. Therefore, 6.74  $M_\odot$  of Fe and 80.2  $M_\odot$  of O are produced by Type II events, whereas 6.53  $M_\odot$  of Fe and 1.45  $M_\odot$  of O are produced by Type Ia events. These assumptions yield 3.10 times more Fe and 2.81 times more O (per star particle) than the ERIS values. For the metallicities and alpha abundances presented in the Letter, we use the more modern relations, which shift the ERIS metallicities by the following amounts:

$$\Delta([\text{Fe}/\text{H}]) = +0.49 \quad \text{and} \quad \Delta([\alpha/\text{Fe}]) = -0.044. \quad (\text{S5})$$

The updated abundance distributions are shown in the bottom panel of Fig. S1 and can be compared to the original distributions in the top panel. The updated abundances are used in all results presented in this Letter.

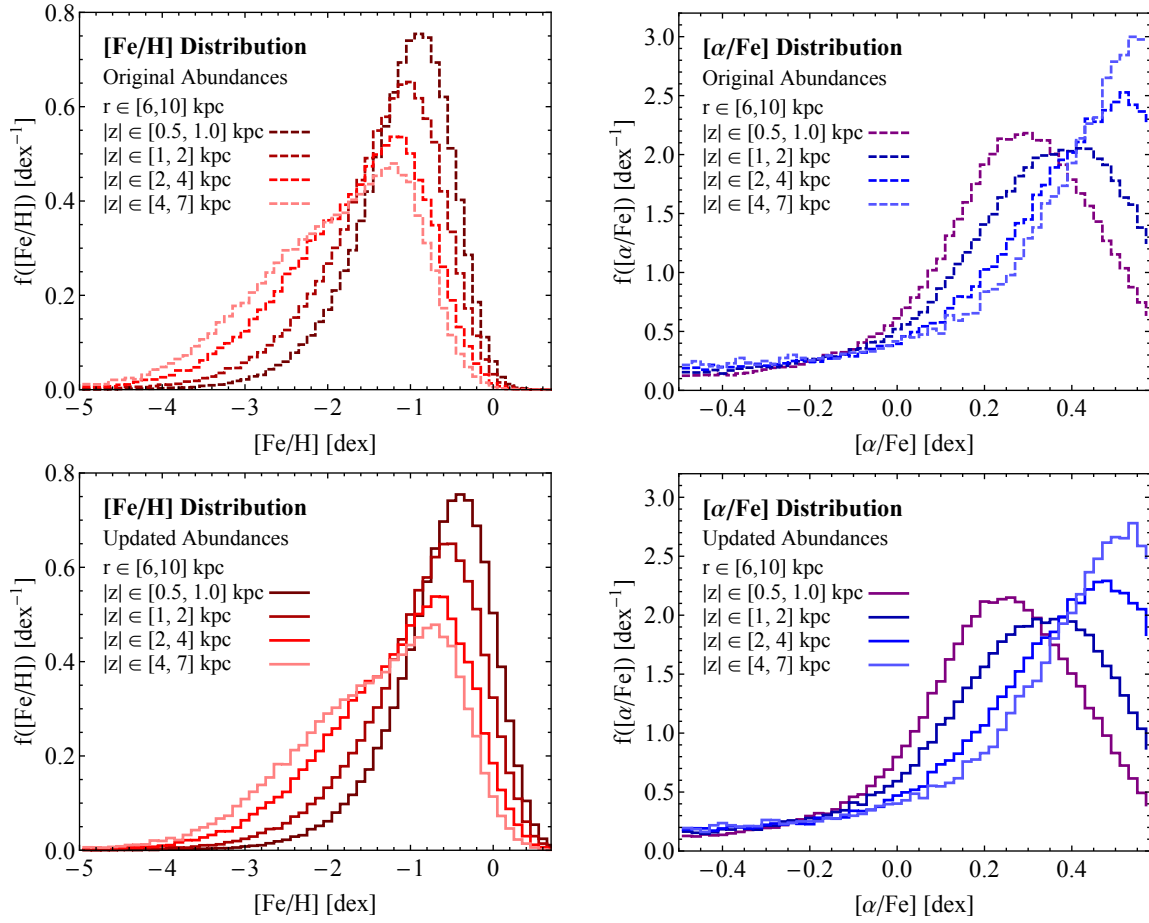


FIG. S1: (Left) Iron abundance  $[\text{Fe}/\text{H}]$  distribution, and (right)  $[\alpha/\text{Fe}]$  distribution of Eris stars within galactocentric radii  $6 \leq r \leq 10$  kpc, as a function of vertical distance off the disk plane. As one moves off the plane, the disk component (centered at  $[\text{Fe}/\text{H}] \sim -0.7$ ) becomes less prominent, and the low-metallicity tail containing the halo stars becomes more pronounced. Similarly, the  $[\alpha/\text{Fe}]$  distribution increases from  $[\alpha/\text{Fe}] \sim 0.2$  to peak around  $[\alpha/\text{Fe}] \sim 0.5$  for higher values of  $z$ . The top row shows the original Eris abundances, while the bottom row shows the updated distributions using a more modern IMF and updated yields. See text for more details.